Nambu-Goldstone mode in a rotating dilute Bose-Einstein condensate

Masahito Ueda[1] and Tatsuya Nakajima[2]
[1]*Department of Physics, Tokyo Institute of Technology, Meguro-ku, Tokyo 152-8551, Japan and ERATO, Japan Science and Technology Corporation (JST), Saitama 332-0012, Japan*
[2]*Physics Department, Graduate School of Science, Tohoku University, Sendai 980-8578, Japan*
(Received 14 November 2003; revised manuscript received 28 December 2005; published 7 April 2006)

The Nambu-Goldstone mode (NGM), associated with vortex nucleation in a harmonically confined, two-dimensional dilute Bose-Einstein condensate is studied. We argue, based on exact diagonalization calculations, that the NGM manifests in the lowest-lying envelope of the quasidegenerate spectrum that emerges as the vortex is about to enter the condensate. The quasidegenerate states constitute a series of octupole-mode branches that originate primarily from pairwise repulsive interactions between octupole excitations and are distinguished by the number of admixed quadrupolar excitations. As the vortex approaches the center of the condensate and the system's axisymmetry is restored, the NGM becomes massive due to its coupling to higher rotational bands. We clarify the mechanism of this mass acquisition by using a newly developed projection-operator method.

DOI: 10.1103/PhysRevA.73.043603 PACS number(s): 03.75.Kk, 05.30.Jp, 67.40.Db

I. INTRODUCTION

A unique feature of gaseous Bose-Einstein condensates (BECs) is the fine tunability of their interatomic interactions using the Feshbach resonance [1,2]. This degree of freedom can be utilized to explore some unique features of a rotating BEC by making the strength of the interactions close, but not equal, to zero. Then, as the angular momentum (AM) $\hbar L$ of the system increases, the low-lying states of the BEC in a harmonic potential become quasidegenerate [3,4] and hence highly susceptible to symmetry-breaking perturbations. This high susceptibility is considered to be the origin of vortex nucleation. Both experimental [5] and mean-field theoretical studies [6–9] have demonstrated that as L increases, vortices enter the system from the edges of the BEC by spontaneously breaking the system's axisymmetry. A Nambu-Goldstone mode (NGM) must be associated with this axisymmetry breaking, but it has not yet been identified. The purpose of this paper is to reveal the NGM using many-body theory and to show that this mode becomes massive as the vortex approaches the center of the BEC, at which point the axisymmetry of the system is restored. We investigate this problem using both exact diagonalization calculations and an analytic approach based on a newly developed projection-operator method.

We consider a system of N identical bosons, each with mass M, that undergo contact interactions and are confined in a two-dimensional harmonic potential with frequency ω. The Hamiltonian of our system is given by

$$H=\sum_{j=1}^{N}\left(\frac{\mathbf{p}_j^2}{2M}+\frac{M\omega^2}{2}\mathbf{r}_j^2\right)+\frac{2\pi\hbar^2 g}{M}\sum_{j\neq k}\delta(\mathbf{r}_j-\mathbf{r}_k), \tag{1}$$

where $\mathbf{p}_j$ is the momentum of the jth particle, $\mathbf{r}_j\equiv(x_j,y_j)$, and g gives the ratio of the mean-field interaction energy per particle to $\hbar\omega$. In the following we use the complex coordinate $z_j\equiv x_j+iy_j$ and measure the length, energy, and AM in units of $(\hbar/M\omega)^{1/2}$, $\hbar\omega$, and $\hbar$, respectively. The single-particle Hamiltonian H_0 and interaction Hamiltonian V are then given by

$$H_0=\sum_{j=1}^{N}\left(-2\frac{\partial^2}{\partial z_j\partial z_j^*}+\frac{|z_j|^2}{2}\right) \tag{2}$$

and

$$V=2\pi g\sum_{j\neq k}\delta(z_j-z_k), \tag{3}$$

respectively. Throughout this paper we shall work in a subspace of a given angular momentum. When $g\ll 1$, the Hilbert space may be restricted to the space spanned by the basis functions

$$\phi_m(z)=\frac{z^m}{\sqrt{\pi m!}}e^{-|z|^2/2}\quad(m=0,1,2,\ldots), \tag{4}$$

where m is the AM quantum number. In this "lowest-Landau-level" approximation, the field operator can be expanded as

$$\hat{\Psi}(z)=\sum_{m=0}^{\infty}\hat{b}_m\phi_m(z), \tag{5}$$

where $\hat{b}_m$ is the annihilation operator of a boson with AM m. The second-quantized form of V then becomes [10]

$$\hat{V}=g\sum_{m_1,\ldots,m_4}V_{m_1,\ldots,m_4}\hat{b}_{m_1}^{\dagger}\hat{b}_{m_2}^{\dagger}\hat{b}_{m_3}\hat{b}_{m_4}, \tag{6}$$

where

$$V_{m_1,\ldots,m_4}=\frac{\delta_{m_1+m_2,m_3+m_4}(m_1+m_2)!}{2^{m_1+m_2}\sqrt{m_1!m_2!m_3!m_4!}}. \tag{7}$$

We note that if all the particles occupy the same quantum state, say that with $m=0$, the interaction energy is given by $gN(N-1)$. Thus the mean-field interaction energy per particle is on the order of gN.

We study the properties of the system as a function of the angular momentum L. We note that in the lowest-Landau-level approximation, the noninteracting Hamiltonian $\hat{H}_0 = L + N$ becomes a constant of motion for a given L and N and that the dynamics of the system are therefore determined by $\hat{V}$ alone. The lowest-energy state of this system for a given L is referred to as the yrast state. The trace of the yrast state viewed as a function of L is called the yrast line. In the following, we measure the energy of the system from that of the yrast state.

This paper is organized as follows. In Sec. II we use the exact diagonalization method to identify the NGM in a rotating BEC. In Sec. III we develop a projection-operator method to clarify why the NGM becomes massive as L increases to N. We show that this mass acquisition occurs due to the coupling of the NGM to higher-rotational bands. In Sec. IV we summarize the main results of this paper.

II. NAMBU-GOLDSTONE MODE IN A ROTATING BOSE-EINSTEIN CONDENSATE

The Nambu-Goldstone mode should appear when the vortex is about to nucleate, that is, when the axisymmetry of the system is being broken. In this regime ($L \ll N$), the excitation spectrum is divided into two groups having very different energy scales [11]. One group involves excitations whose energies are of the order of gN and the other involves excitations whose energies are of the order of g. The latter group originates primarily from pairwise repulsive interactions between octupole modes with an excitation spectrum given by [11]

$$\hat{O} = \frac{27g}{34}\hat{b}_3^\dagger \hat{b}_3(\hat{b}_3^\dagger \hat{b}_3 - 1). \tag{8}$$

Because the energy scale ($\sim g$) of the latter group is smaller than that of the former, by a factor of $1/N$, and hence vanishes in the thermodynamic limit, it might be supposed that $\hat{O}$ describes the NGM. However, this is not the case. We show that the NGM manifests in the states in the envelope of equally spaced octupole-mode branches that are generated by the admixture of quadrupole-mode excitations to the states described by Eq. (8). The envelope is labeled **G** in Fig. 1 and is obtained by exact diagonalization of $\hat{V}$ for $N=256$. This envelope structure has not been found previously because it emerges only for large N and for relatively large values of L/N [12]. In Fig. 1, octupole-mode branches are indicated by solid and dotted curves, which are equally spaced with $\Delta L = 2$. We have confirmed that this spacing corresponds to the admixture of one quadrupole-mode excitation.

For a mode to qualify as a NGM, it must meet three conditions: it must be massless, it must be associated with a broken symmetry, and it must restore the broken symmetry. Here by massless we mean that the excitation energy vanishes in the thermodynamic limit. Because the **G** mode belongs to the second group mentioned above, i.e., with excitation energies of the order of g, the excitation energy of the **G** mode vanishes in the thermodynamic limit, thus meeting the first condition. Since the yrast states for $L \leqslant N$ are energetically degenerate under rotation with angular velocity $\Omega = \partial E_{\mathrm{tot}}/\partial L = \omega(1 - gN/2)$, axisymmetry breaking is expected to occur for an infinitesimal, axisymmetry-breaking perturbation. In fact, mean-field theory predicts [6] that as the vortex enters the system, the axisymmetry of the density profile is spontaneously broken, as illustrated in Fig. 2. Thus the second condition is met. Since the symmetry-restoring force is a correction to the mean-field result, we invoke the many-body theory to determine whether or not the third condition is met.

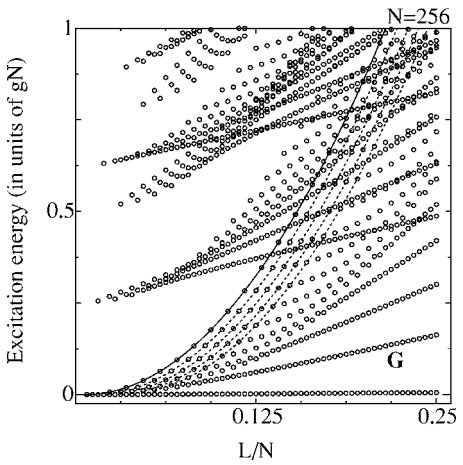

FIG. 1. Many-body energy spectrum of $\hat{V}$ of Eq. (6) with $N = 256$. The energy is measured from the yrast line (horizontal bottom line) and excited states that involve center-of-mass motion are not shown. The solid and dotted curves are obtained from least-squares fits of the data to quadratic polynomials. The solid curve shows the branch that arises from pairwise repulsive interactions between octupole-mode excitations alone and is well described by Eq. (8). The dotted curves are displaced from the solid curve by 2, 4, 6, and 8 units of angular momentum. These shifts are caused by the admixture of 1, 2, 3, and 4 quadrupole-mode excitations, respectively. The envelope of lowest-lying excited states is labeled **G**, for which the Nambu-Goldstone mode manifests. As L increases, the envelope develops an energy gap on the order of N, indicating mass acquisition by the Nambu-Goldstone mode.

We note that in exact diagonalization calculations the single-particle density-distribution function

$$\rho(\mathbf{r}) = \langle \hat{\Psi}^\dagger(\mathbf{r})\hat{\Psi}(\mathbf{r})\rangle, \tag{9}$$

is isotropic [i.e., $\rho(\mathbf{r}) = \rho(|\mathbf{r}|)$] and is not suitable for studying the problem of axisymmetry breaking. Symmetry breaking can be studied with the conditional distribution function (CDF) [13] defined as

$$\rho(\mathbf{r};\mathbf{r}_0) = \frac{1}{\rho(\mathbf{r}_0)}\langle \hat{\Psi}^\dagger(\mathbf{r})\hat{\Psi}^\dagger(\mathbf{r}_0)\hat{\Psi}(\mathbf{r}_0)\hat{\Psi}(\mathbf{r})\rangle, \tag{10}$$

where $\mathbf{r}_0$ is the position of a test particle, which we assume without loss of generality to be located on the x axis, i.e., $\mathbf{r}_0 = (r_0, 0)$. Here the test particle should be placed well outside of the border of the condensate $|\mathbf{r}| \simeq 1$, so that a mixing of effects due to pair repulsion between atoms and vortex structure is negligible. In the following discussion we therefore take $r_0 = 3$. Here, by negligible we mean that $\rho(|\mathbf{r}|)$ is not

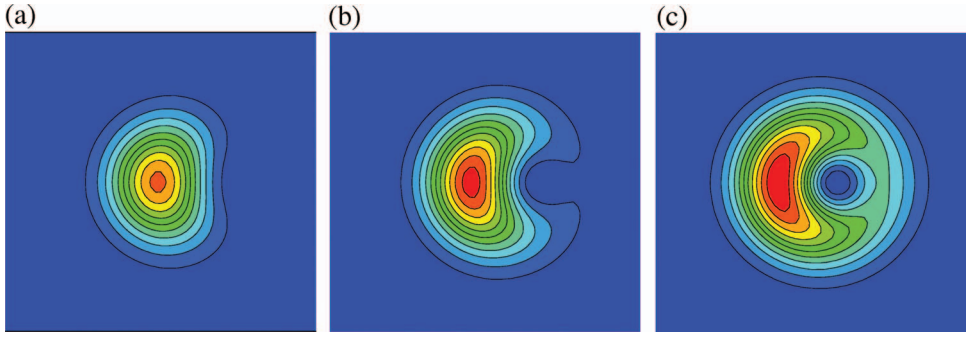

FIG. 2. (Color) Mean-field density profiles of BEC for (a) $L/N=0.125$, (b) $L/N=0.5$, and (c) $L/N=0.875$.

affected by putting the test particle at $\mathbf{r}_0$. The test particle thus acts as an infinitesimal symmetry-breaking perturbation on the two-body correlation function.

In a harmonic potential, the single-particle density-distribution function $\rho(|\mathbf{r}|)$ varies in space. To subtract this single-particle part of the variation from the CDF, we define

$$\tilde{\rho}(\mathbf{r};\mathbf{r}_0) \equiv \frac{N}{N-1}\rho(\mathbf{r};\mathbf{r}_0) - \rho(|\mathbf{r}|). \tag{11}$$

For later use, we define the Fourier components C_m of $\tilde{\rho}$ as

$$\tilde{\rho}(\mathbf{r};\mathbf{r}_0) = \sum_{m=0}^{\infty} C_m(r;|\mathbf{r}_0|)\frac{\cos(m\theta)}{\sqrt{\pi}}, \tag{12}$$

where r and θ are the polar coordinates of $\mathbf{r}$. Only the cosine terms appear in the expansion because of the reflection symmetry of $\tilde{\rho}$ against $\theta \to -\theta$.

Figure 3 illustrates the CDF $\tilde{\rho}(\mathbf{r};|\mathbf{r}_0|=3)$ for the yrast states of 76 bosons with $L=6$, 9, and 12. Figure 3(a) exhibits twofold symmetry, reflecting the fact that the AM of the yrast state is carried mostly by quadrupole-mode excitations. At this stage the vortex is not yet nucleated and the AM is carried by rotation of the entire condensate which is deformed in a quadrupolar manner. As the AM increases, the CDF develops a dip, indicating the entrance of the vortex from the positive X direction.

We note that for $L/N \ll 1$ one of the peaks is located near the boundary of the condensate where the vortex enters. This implies that for $L/N \ll 1$ the quadrupole-mode excitations compensate for the density depletion caused by the entrance of the vortex in the same way that the octupole-mode excitations do (as discussed below).

Figure 4 illustrates the CDF for the first excited states with $L=6$, 12, and 30. The CDF in Fig. 4(a) exhibits threefold symmetry, reflecting the fact that the AM of the first excited states is carried mostly by octupole-mode excitations. It should be noted that one of the peaks is located near the boundary of the condensate where the vortex enters. This implies that the octupole-mode excitations compensate for the density depletion caused by the entrance of the vortex, thus restoring the axisymmetry of the system. A further increase in L is caused by quadrupole-mode excitations (the dotted curves in Fig. 1), so that the lowest-lying excited state gradually loses its threefold symmetry, as illustrated in Fig. 4(b). For larger values of L the CDF eventually shows a dipolelike structure, as shown in Fig. 4(c). On the other hand, the yrast state gradually loses its twofold symmetry [Fig. 3(b)] and the CDF of the yrast state at $L=12$ features a dipolelike structure [Fig. 3(c)]. The dipolelike distribution signifies the entrance of the first vortex into the condensate by breaking the axisymmetry of the system.

Figures 5(a), 5(b), and 5(c) show the Fourier coefficients $C_m(r;|\mathbf{r}_0|=3)$ of Eq. (12) for $m=1$, 2, and 3, respectively, for the lowest-lying excited states, which constitute the **G** branch in Fig. 1. We note that $C_1(r;|\mathbf{r}_0|=3)$ is negative with a large magnitude around $r=1$ (i.e., around the periphery of the condensate), which implies that this component is responsible for the entry of the vortex. On the other hand, the signs of $C_m(r;|\mathbf{r}_0|=3)$ for $m=2$ and $m=3$ are positive for $L \ll N$ and their magnitudes are maximal around $r=1$. This implies that these two modes cooperate with each other to counteract the density depletion caused by the entrance of the vortex, in agreement with what is stated above. We note that the amplitudes of C_2 and C_3 dwindle rapidly and that C_2 changes its sign when L increases beyond the quasidegenerate region. We have confirmed that the signs of C_4 and C_5 are also positive, but that their magnitudes are negligibly small

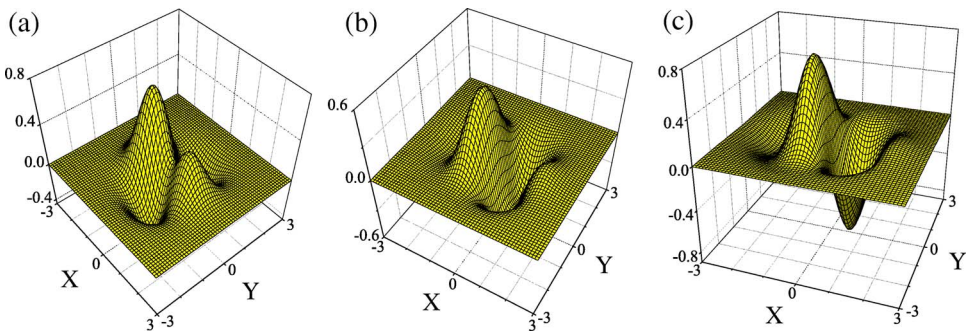

FIG. 3. (Color online) Conditional distribution functions $\tilde{\rho}(\mathbf{r};|\mathbf{r}_0|=3)$ defined by Eq. (12) for the yrast states with (a) $L=6$, (b) $L=9$, (c) $L=12$. The number of bosons is 76 and the test particle is placed at $\mathbf{r}_0=(3,0)$.

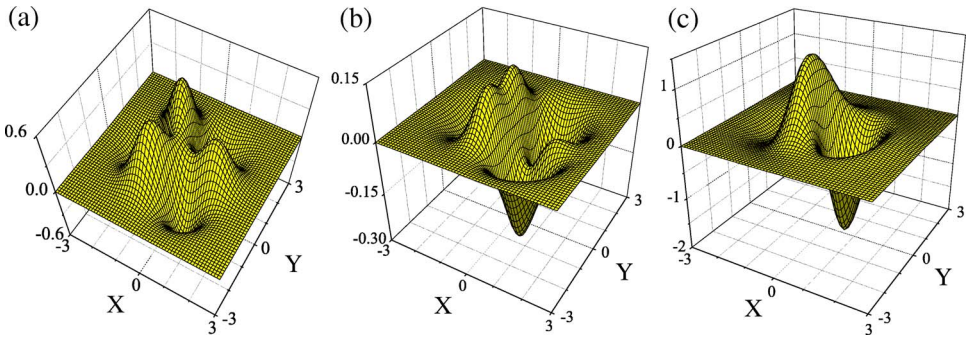

FIG. 4. (Color online) Conditional distribution functions $\tilde{\rho}(\mathbf{r};|\mathbf{r}_0|=3)$ for the lowest-lying excited states with (a) $L=6$, (b) $L=12$, (c) $L=30$. The number of bosons is 76 and the test particle is placed at $\mathbf{r}_0=(3,0)$.

compared with that of C_3. This also supports our claim that the modes with $m=2$ and $m=3$ constitute the NGM.

III. MASS ACQUISITION OF THE NAMBU-GOLDSTONE MODE

The NGM, which is labeled as **G** in Fig. 1, is massless only in the regime $L \ll N$. We note that the same branch acquires a finite energy gap proportional to N as L approaches N, that is, the NGM becomes massive. Physically, this is because the axisymmetry is restored as the vortex reaches the center of BEC. In this section we consider the mechanism by which the NGM becomes massive as L increases. Because the center-of-mass (c.m.) motion in the harmonic potential is decoupled from the other degrees of freedom, we can separate the coordinates into the c.m. coordinate

$$z_c = \frac{1}{N}\sum_{j=1}^{N} z_j \tag{13}$$

and the relative coordinates $u_j \equiv z_j - z_c$, where

$$\sum_{i=1}^{N} u_i = 0. \tag{14}$$

The total Hamiltonian can then be decomposed into a c.m. component $H^{\text{c.m.}}$ and a relative component $H^{\text{rel}}+V$, where

$$H^{\text{c.m.}} = -\frac{2}{N}\frac{\partial^2}{\partial z_c \partial z_c^*} + \frac{N}{2}|z_c|^2, \tag{15}$$

$$H^{\text{rel}} = \frac{2}{N}\sum_{j,k=1}^{N-1}(1-N\delta_{jk})\frac{\partial^2}{\partial u_j \partial u_k^*} + \frac{1}{2}\sum_{j=1}^{N}|u_j|^2, \tag{16}$$

$$V = 2\pi g \sum_{j\neq k}\delta(u_j - u_k). \tag{17}$$

Accordingly, a many-body wave function can be separated into the counterparts:

$$\Psi(z_1,\ldots,z_N) = \Psi^{\text{c.m.}}(z_c)\Psi^{\text{rel}}(u_1,\ldots,u_{N-1}). \tag{18}$$

The Schrödinger equation for $H^{\text{c.m.}}$

$$H^{\text{c.m.}}\Psi_m^{\text{c.m.}} = \epsilon_m^{\text{c.m.}}\Psi_m^{\text{c.m.}},$$

can easily be solved, giving the eigenenergies

$$\epsilon_m^{\text{c.m.}} = m+1 \quad (m=0,1,2,\ldots),$$

and the corresponding eigenfunctions

$$\Psi_m^{\text{c.m.}}(z_c) = \sqrt{\frac{N^{m+1}}{\pi m!}} z_c^m e^{-(N/2)|z_c|^2}.$$

To solve the Schrödinger equation for H^{rel}

$$H^{\text{rel}}\Psi^{\text{rel}} = \epsilon^{\text{rel}}\Psi^{\text{rel}},$$

we put $\Psi^{\text{rel}} = f e^{-(1/2)\Sigma_{j=1}^{N}|u_j|^2}$, obtaining

$$\sum_{j=1}^{N-1}\left(u_j\frac{\partial}{\partial u_j} + u_j^*\frac{\partial}{\partial u_j^*} - 2\frac{\partial^2}{\partial u_j \partial u_j^*}\right)f + \frac{2}{N}\sum_{j,k=1}^{N-1}\frac{\partial^2 f}{\partial u_j \partial u_k^*} = [\epsilon^{\text{rel}} - (N-1)]f. \tag{19}$$

The ground state corresponds to constant f which gives

$$\epsilon_0^{\text{rel}} = N-1 \tag{20}$$

and

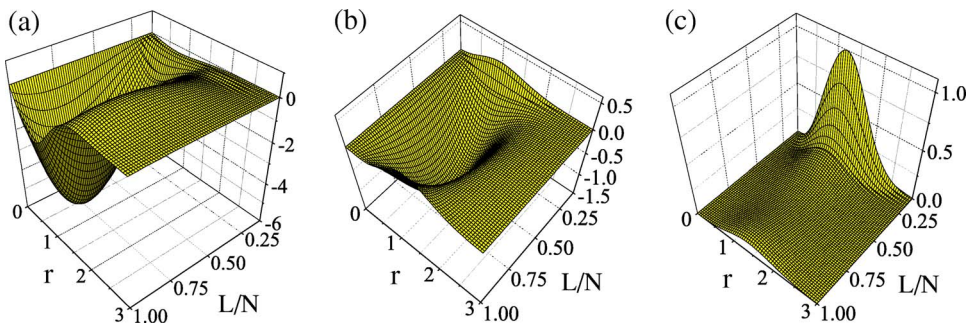

FIG. 5. (Color online) Expansion coefficients $C_m(r;|\mathbf{r}_0|=3)$ for (a) $m=1$, (b) $m=2$, and (c) $m=3$, shown for the lowest-lying excited state for each L satisfying $8 \leqslant L \leqslant N=76$. The test particle is placed at $\mathbf{r}_0=(3,0)$.

$$\Psi^{\mathrm{rel}} = \frac{1}{\sqrt{N\pi^{N-1}}} e^{-(1/2)\Sigma_{i=1}^{N}|u_i|^2}.$$

The right-hand side of Eq. (20) represents the zero-point energy of the system minus the zero-point energy of the c.m. motion.

In the lowest-Landau-level approximation, f does not depend on u_j^* and Eq. (19) reduces to

$$\sum_{j=1}^{N-1} u_j \frac{\partial f}{\partial u_j} = [\epsilon^{\mathrm{rel}} - (N-1)]f. \tag{21}$$

When the total AM of the system is L, the general solution to Eq. (21) is given by

$$f_L = \sum{}' C_{m_1,\ldots,m_{N-1}} u_1^{m_1} \cdots u_{N-1}^{m_{N-1}}, \tag{22}$$

where the primed sum runs over all possible nonnegative integers of m_j subject to the constraint $\Sigma_{j=1}^{N-1} m_j = L$. Bose symmetry requires that the coefficients $C_{m_1,\ldots,m_{N-1}}$ be symmetric under exchange of any two arguments:

$$C_{\ldots,m_i,\ldots,m_j,\ldots} = C_{\ldots,m_j,\ldots,m_i,\ldots}.$$

Thus f is a symmetric polynomial of order L. In the following we focus only on this polynomial part and omit the exponential part $e^{-(1/2)\Sigma_{i=1}^{N}|u_i|^2}$.

The most even way to distribute L ($\leqslant N$) units of AM over N particles is to assign one unit to each of L particles and then sum over all possible choices of L particles from a total of N particles with equal weight

$$Y_L = \sum_{1 \leqslant i_1 < i_2 < \cdots < i_L \leqslant N} u_{i_1} u_{i_2} \cdots u_{i_L}, \tag{23}$$

where the sum runs over all integers $i_1, i_2, \ldots, i_L$ that satisfy $1 \leqslant i_1 < i_2 < \cdots < i_L \leqslant N$. We define $Y_0 = 1$ and note that $Y_1 = 0$, due to Eq. (14). The state (23), referred to as the yrast state, is the lowest-energy state of the system subject to a given AM L, and it satisfies [10,14] (see also Appendix A)

$$VY_L = gN\left(N - 1 - \frac{L}{2}\right) Y_L. \tag{24}$$

To analyze low-lying excited states above the yrast state, we introduce a projection operator e_i, the action of which is to eliminate those terms that contain the factor u_i in the operand. For example,

$$e_i u_j = (1 - \delta_{ij}) u_j,$$

$$(1 - e_i) u_j = \delta_{ij} u_i,$$

$$e_i u_j u_k = (1 - \delta_{ij})(1 - \delta_{ik}) u_j u_k. \tag{25}$$

We also note that the identity operator can be decomposed as follows:

$$1 = e_i e_j + e_i(1 - e_j) + (1 - e_i) e_j + (1 - e_i)(1 - e_j). \tag{26}$$

This decomposition will be used later. Many-body wave functions can be constructed in a systematic way by the appropriate operation of e_i on the yrast-state wave function (23). The low-lying excitations of interacting Bose systems are collective in nature [4]; we claim that the main features of the excitation spectrum (i.e., the large energy gap of the **G** mode for large L and the almost linear high-lying rotational bands) arise from a particular set of coupled collective excitations generated by the operators

$$P_m = \sum_{i=1}^{N} u_i^m e_i \quad (m = 0, 1, \ldots). \tag{27}$$

These operators are analogous to Mottelson's multipolar operators $Q_m \propto \Sigma_i z_i^m$ [4] but differ in that z_i is replaced by u_i and that the projection operator e_i is incorporated. Both of these modifications are essential for identifying an invariant subspace spanned by the yrast states and for constructing the desired many-body excited states above the yrast state.

We consider a linear superposition of the states

$$M_L^{(m)} \equiv P_m Y_{L-m} \quad (m = 3, 4, \ldots, L), \tag{28}$$

where $M_L^{(m)}$ describes an excitation in which one particle carries an AM of m and $L-m$ particles each carry a unit of AM:

$$M_L^{(m)} = \sum_{i_1 < \cdots < i_{L-m+1}} \sum_{k=1}^{L-m+1} u_{i_k}^{m-1} \prod_{l=1}^{L-m+1} u_{i_l}. \tag{29}$$

The remaining $N-L+m-1$ particles carry no AM and thus the condition $L \leqslant N+m-1$ must be met. Our strategy is to seek an approximate eigenstate spanned by Y_L and $M_L^{(m)}$. Toward this end, we should understand how they are transformed under application of V. Because the yrast state has an eigenenergy given by Eq. (24), it is convenient to define

$$g\tilde{V} \equiv V - gN\left(N - 1 - \frac{L}{2}\right). \tag{30}$$

Then

$$\tilde{V} Y_L = 0. \tag{31}$$

The transformation law of $M_L^{(m)}$ under the application of $\tilde{V}$ is given (for details, see Appendix B) as

$$\begin{aligned}\tilde{V} M_L^{(m)} = \frac{1}{2}\{&(m + 2^{3-m} - 4)N + [2^{2-m}(m-1) + 1] \\ &\times (L - m) + 4(1 - 2^{1-m})\} M_L^{(m)} - \frac{1}{2}(1 - 2^{2-m}) \\ &\times (N - L + m) M_L^{(m+1)} + 2^{2-m} m (L - m + 1) \\ &\times M_L^{(m-1)} + R_{m+1} + R_m,\end{aligned} \tag{32}$$

where $\theta(k \geqslant l) = 1$ if $k \geqslant l$ and $\theta(k \geqslant l) = 0$ otherwise, and

$$R_m = \theta(m \geqslant 4) \sum_{k=2}^{m-2} \frac{2^{1-m} m!}{k!(m-k)!} P_{m-k} M_{L-m+k}^{(k)}. \tag{33}$$

Equation (32), together with Eq. (33), is the desired recursion relation. We see that each mode described by $M_L^{(m)}$ is coupled with other modes $M_L^{(k)}$ with $k = 3, 4, \ldots, m-1$ and $k = m+1$. Since the coefficient of $M_L^{(m+1)}$ in Eq. (32) includes

the factor $N-L+m$, the weight of this term decreases monotonically with increasing L. By introducing the truncation approximation discussed below and ignoring contributions from higher-order terms such as $M_l^{(l)}M_{L-l}^{(m)}$, we obtain a closed set of linear equations that can be solved easily even for a large value of m. It turns out that to quantitatively reproduce the **G** mode in Fig. 1, we must take into account values of m up to relatively large values, e.g., up to 7, because higher rotational bands couple strongly to the **G** mode, as discussed below. Writing Eq. (32) explicitly for $m=3,\ldots,7$, we obtain

$$\tilde{V}M_L^{(3)} = \frac{1}{4}(4L-9)M_L^{(3)} - \frac{N-L+3}{4}M_L^{(4)} - \frac{3}{4}L(L-2)Y_L,$$

$$\tilde{V}M_L^{(4)} = -\frac{L}{4}M_L^{(3)} + \frac{2N+7L-24}{8}M_L^{(4)} - \frac{3}{8}(N-L+4)M_L^{(5)} + \frac{3}{4}L(L-2)Y_L,$$

$$\tilde{V}M_L^{(5)} = -\frac{5}{8}(L-3)M_L^{(3)} - \frac{5}{16}(L-2)M_L^{(4)} + \frac{10N+12L-55}{16}M_L^{(5)} - \frac{7}{16}(N-L+5)M_L^{(6)},$$

$$\tilde{V}M_L^{(6)} = -\frac{15}{32}(L-3)M_L^{(3)} - \frac{15}{32}(2L-7)M_L^{(4)} - \frac{3}{32}(3L-10)M_L^{(5)} + \frac{34N+21L-120}{32}M_L^{(6)} - \frac{15}{32}(N-L+6)M_L^{(7)},$$

$$\tilde{V}M_L^{(7)} = -\frac{7}{32}(L-3)M_L^{(3)} - \frac{7}{64}(5L-18)M_L^{(4)} - \frac{21}{64}(2L-9)M_L^{(5)} - \frac{7}{64}(2L-9)M_L^{(6)} - \frac{98N+38L-259}{64}M_L^{(7)} - \frac{31}{64}(N-L+7)M_L^{(8)}. \tag{34}$$

We note that the diagonal coefficients of $M_L^{(m)}$ for $m=4$ and 5 are $(2N+7L-24)/8$ and $(10N+12L-55)/16$, respectively, and that they reproduce rather well the almost linear spectra in Fig. 6. We refer to these as higher rotational bands. We also note the coupling of $M_L^{(m)}$ $(m\geqslant 4)$ to $M_L^{(3)}$ becomes very strong, on the order of $O(N)$, near $L\sim N$. To reproduce the lowest-lying branch consisting mainly of $M_L^{(3)}$, we therefore have to solve the coupled equations for $m=3,4,\ldots$. By ignoring the last term with $M_L^{(8)}$, the set of equations in Eq. (34) is closed and can be solved with the condition of Eq. (31) in a straightforward manner. The solid curve in Fig. 6 shows the lowest excitation energy obtained by solving the above closed set of equations. This curve matches the **G** mode rather well.

These considerations clearly show that the mechanism of mass acquisition of the NGM with increasing L is due to its coupling to higher rotational bands, whose coupling constants grow with L. Physically, this appears quite natural because as L approaches N, the axisymmetry of the system, which is spontaneously broken upon vortex nucleation, is almost fully recovered and hence the NGM should disappear.

IV. SUMMARY

In this paper we investigated the Nambu-Goldstone mode (NGM) associated with vortex nucleation in a two-dimensional Bose-Einstein condensate by using the numerical diagonalization method and an analytic approach based on a projection-operator method. Mean-field theory predicts that the axisymmetry of the system is spontaneously broken when the vortex enters the system, as shown in Fig. 2. However, the NGM associated with this axisymmetry breaking

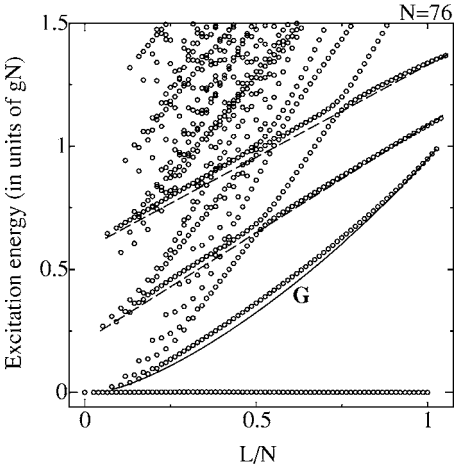

FIG. 6. Comparison between the excitation energy of the **G** mode obtained by solving a set of linearized equations for $m=3,4,\ldots,7$ (solid curve) and that obtained by the exact diagonalization of the Hamiltonian (open circles) for $N=76$. The dashed lines describe $(2N+7L-24)/8$ and $(10N+12L-55)/16$, which are the diagonal coefficients of $M_L^{(m)}$ in Eq. (34) for $m=4$ and 5, respectively (see text). The energy is measured from the yrast state, which corresponds to the horizontal bottom line.

had been elusive. We claim that the NGM manifests in the lowest-lying envelope of a series of octupole-mode branches that are shifted from each other by admixtures of quadrupole-mode excitations. This mode, which is denoted as **G** in Figs. 1 and 6, possesses all the properties required for it to qualify as the NGM: (1) it is associated with the axisymmetry breaking, (2) it is a zero mode whose excitation energy is of the order of $1/N$ and therefore vanishes in the thermodynamic limit, and (3) it restores the broken axisymmetry.

As shown in Fig. 6, the excitation energy of the **G** mode becomes of the order of gN which therefore does not vanish in the thermodynamic limit. The NGM thus becomes massive as L approaches N. We have developed a projection-operator method to show that this mass acquisition occurs due to coupling of the NGM to higher rotational bands.

ACKNOWLEDGMENTS

M.U. and T.N. acknowledge support by Grants-in-Aid for Scientific Research (Grant Nos. 15340129, 17071005, and 16740164) from the Ministry of Education, Culture, Sports, Science, and Technology of Japan. M.U. acknowledges support by a CREST program of the JST.

APPENDIX A: PROPERTIES OF THE MANY-BODY WAVE FUNCTION Y_L OF THE YRAST STATE

We first note the following relation:

$$\sum_{i_1<\cdots<i_L}\sum_{k=1}^{L}\delta_{i,i_k}u_{i_1}\cdots u_{i_L}=u_ie_iY_{L-1}. \tag{A1}$$

This can be proved by carrying out the sum over k and taking out the common factor u_i.

By applying Eq. (25) repeatedly, we obtain

$$\begin{aligned}e_iY_L&=\sum_{i_1<\cdots<i_L}(1-\delta_{ii_1})\cdots(1-\delta_{ii_L})u_{i_1}\cdots u_{i_L}\\&=\sum_{i_1<\cdots<i_L}\left[1-\sum_{k=1}^{L}\delta_{i,i_k}\right]u_{i_1}\cdots u_{i_L}=Y_L-u_ie_iY_{L-1},\end{aligned} \tag{A2}$$

where Eq. (A1) is used in deriving the last equality. Thus we have

$$(1-e_i)Y_L=u_ie_iY_{L-1}. \tag{A3}$$

Summing both sides of Eq. (A2) over i and using the relation $\Sigma_{i=1}^{N}\Sigma_{k=1}^{L}\delta_{ii_k}=L$, we obtain

$$\sum_i e_iY_L=(N-L)Y_L. \tag{A4}$$

Equation (A3) can be used to derive

$$\sum_i u_ie_iY_{L-1}=\sum_i(1-e_i)Y_L=NY_L-\sum_i e_iY_L$$

which, together with Eq. (A3), gives

$$\sum_i u_ie_iY_{L-1}=LY_L. \tag{A5}$$

In a similar manner, we may derive various formulas. Here we list some of the formulas that are relevant to this paper

$$\sum_i u_i^2e_iY_{L-1}=-LY_L, \tag{A6}$$

$$\sum_{i\neq j}u_iu_je_ie_jY_{L-2}=L(L-1)Y_L. \tag{A7}$$

As an illustrative example, we prove Eq. (24) (see also Ref. [14]). Applying the operator of Eq. (26) to Y_L and using the relations of Eq. (25) we obtain for $i\neq j$

$$Y_L=e_ie_jY_L+(u_i+u_j)e_ie_jY_{L-1}+u_iu_je_ie_jY_{L-2}. \tag{A8}$$

Applying the operator $2\pi\delta(u_i-u_j)$ to both sides of Eq. (A8) gives

$$\begin{aligned}2\pi\delta(u_i-u_j)Y_L&=e_ie_jY_L+(u_i+u_j)e_ie_jY_{L-1}\\&\quad+\frac{(u_i+u_j)^2}{4}e_ie_jY_{L-2}\\&=Y_L+\frac{(u_i-u_j)^2}{4}e_ie_jY_{L-2},\end{aligned}$$

where we have used $u_i,\ u_j\to(u_i+u_j)/2$ under the application of $2\pi\delta(u_i-u_j)$. Summing both sides over i and j gives

$$\begin{aligned}VY_L&=N(N-1)Y_L+\sum_{i\neq j}\frac{(u_i-u_j)^2}{4}e_ie_jY_{L-2}\\&=N(N-1)Y_L+\frac{1}{2}\sum_{i\neq j}(u_i^2-u_iu_j)e_ie_jY_{L-2}.\end{aligned}$$

Substituting Eqs. (A6) and (A7) into the right-hand side of this equation proves Eq. (24).

APPENDIX B: DERIVATION OF EQ. (32)

Applying the operator of Eq. (26) to $M_L^{(m)}$ gives

$$\begin{aligned}M_L^{(m)}&=e_ie_jM_L^{(m)}+(u_i+u_j)e_ie_jM_{L-1}^{(m)}+(u_i^m+u_j^m)e_ie_jY_{L-m}\\&\quad+u_iu_je_ie_jM_{L-2}^{(m)}+(u_i^mu_j+u_iu_j^m)e_ie_jY_{L-m-1}.\end{aligned}$$

The application of $2\pi\delta(u_i-u_j)$ on both sides gives

$$\begin{aligned}2\pi\delta(u_i-u_j)M_L^{(m)}&=M_L^{(m)}+\frac{(u_i-u_j)^2}{4}e_ie_jM_{L-2}^{(m)}\\&\quad+\left[\frac{(u_i+u_j)^m}{2^{m-1}}-(u_i^m+u_j^m)\right]e_ie_jY_{L-m}\\&\quad+\left[\frac{(u_i+u_j)^{m+1}}{2^m}-(u_i^mu_j\right.\\&\quad\left.+u_iu_j^m)\right]e_ie_jY_{L-m-1}.\end{aligned}$$

Summing both sides of this equation over i and $j(\neq i)$, we obtain for $m\leqslant 3$

$$\tilde{V}M_L^{(m)} = A_m + B_m + C_m, \tag{B1}$$

where

$$A_m = \frac{NL}{2}M_L^{(m)} + \frac{1}{4}\sum_{i\neq j}(u_i - u_j)^2 e_i e_j M_{L-2}^{(m)},$$

$$B_m = \sum_{i\neq j}\left[\frac{(u_i+u_j)^m}{2^{m-1}} - (u_i^m + u_j^m)\right] e_i e_j Y_{L-m},$$

$$C_m = \sum_{i\neq j}\left[\frac{(u_i+u_j)^{m+1}}{2^m} - (u_i^m u_j + u_i u_j^m)\right] e_i e_j Y_{L-m-1}. \tag{B2}$$

These quantities can be calculated by expanding the right-hand sides and evaluating each term. This can be carried out by using the following identities, which can be proved in a manner similar to that described in Appendix A:

$$\sum_i e_i M_L^{(m)} = (N - L + m - 1)M_L^{(m)},$$

$$\sum_i u_i e_i M_{L-1}^{(m)} = (L - m)M_L^{(m)},$$

$$\sum_i u_i^2 e_i M_{L-2}^{(m)} = -(L - m)M_L^{(m)} - M_L^{(m+1)},$$

$$\sum_i u_i^k e_i M_{L-k}^{(m)} = [(N-1)\delta_{k0} + (-1)^{k-1}(L-m)]M_L^{(m)} + \theta(k \geqslant 2)\sum_{l=1}^{k-1}(-1)^{k+l}M_L^{(m+l)} + \theta(k \geqslant 3)\sum_{l=2}^{k-1}(-1)^{k+l-1}M_l^{(l)}M_{L-l}^{(m)} + \theta(k \geqslant 2)(-1)^k\sum_i u_i M_{L-1}^{(m)},$$

where $\theta(k \geqslant l) = 1$ if $k \geqslant l$ and $\theta(k \geqslant l) = 0$ otherwise. We may use these relations to calculate A_m, B_m, and C_m in Eq. (B2). The results are given by

$$A_m = \frac{1}{2}(mN + L - m)M_L^{(m)} - \frac{1}{2}(N - L + m)M_L^{(m+1)},$$

$$B_m = 2(2^{1-m} - 1)(N - L + m - 1)M_L^{(m)} + 2^{2-m}m(L - m + 1)M_L^{(m-1)} + R_m,$$

$$C_m = 2^{1-m}(N - L + m)M_L^{(m+1)} + 2[2^{-m}(m+1) - 1](L - m)M_L^{(m)} + R_{m+1},$$

where R_m is given by Eq. (33). Substituting these into Eq. (B1) proves Eq. (32).

[1] S. Inouye, M. R. Andrews, J. Stenger, H.-J. Miesner, D. M. Stamper-Kurn, and W. Ketterle, Nature (London) **392**, 151 (1998).

[2] S. L. Cornish, N. R. Claussen, J. L. Roberts, E. A. Cornell, and C. E. Wieman, Phys. Rev. Lett. **85**, 1795 (2000).

[3] N. K. Wilkin, J. M. F. Gunn, and R. A. Smith, Phys. Rev. Lett. **80**, 2265 (1998).

[4] B. Mottelson, Phys. Rev. Lett. **83**, 2695 (1999).

[5] K. W. Madison, F. Chevy, W. Wohlleben, and J. Dalibard, Phys. Rev. Lett. **84**, 806 (2000).

[6] D. A. Butts and D. S. Rokhsar, Nature (London) **397**, 327 (1999).

[7] S. Sinha and Y. Castin, Phys. Rev. Lett. **87**, 190402 (2001).

[8] M. Tsubota, K. Kasamatsu, and M. Ueda, Phys. Rev. A **65**, 023603 (2002).

[9] M. Kramer, L. Pitaevskii, S. Stringari, and F. Zambelli, Laser Phys. **12**, 113 (2002).

[10] G. F. Bertsch and T. Papenbrock, Phys. Rev. Lett. **83**, 5412 (1999).

[11] T. Nakajima and M. Ueda, Phys. Rev. A **63**, 043610 (2001); M. Ueda and T. Nakajima, *ibid.* **64**, 063609 (2001); G. M. Kavoulakis, B. Mottelson, and C. J. Petnick, *ibid.* **62**, 063605 (2000); G. M. Kavoulakis, B. Mottelson, and S. M. Reimann, *ibid.* **63**, 055602 (2001); V. Bardek, L. Jonke, and S. Meljanac, *ibid.* **64**, 015603 (2001); V. Bardek and S. Meljanac, *ibid.* **65**, 013602 (2002).

[12] In a previous paper [T. Nakajima and M. Ueda, Phys. Rev. Lett. **91**, 140401 (2003)], we reported the results of similar exact diagonalization calculations for $N=25$. However, this size is too small to reveal the structure of a quasi-degenerate spectrum on the order of g, and thus we could not distinguish the NGM from the yrast line. However, if we restrict L to $L \ll N$, we can perform exact diagonalization calculations for a much larger N, say, $N=10\,000$, though we are then not able to cover L up to $L/N \sim 0.1$, which is necessary to investigate how the NGM becomes massive with increasing L.

[13] X.-J. Liu, H. Hu, L. Chang, W. Zhang, S.-Q. Li, and Y.-Z. Wang, Phys. Rev. Lett. **87**, 030404 (2001).

[14] R. A. Smith and N. K. Wilkin, Phys. Rev. A **62**, 061602(R) (2000); T. Papenbrock and G. F. Bertsch, *ibid.* **63**, 023616 (2001).